Soft Matter

PAPER

View Article Online
View Journal | View Issue

Cite this: *Soft Matter*, 2025, **21**, 6779

Stabilizing light-responsive azobenzene films in an aqueous environment with thin polymer coatings

Mari Isomäki,[a] Lotta Kääriäinen,[a] Chiara Fedele,*[a] Suvi Lehtimäki,[a] Tero-Petri Ruoko,[a] Elina Mäntylä,[b] Teemu O. Ihalainen[b] and Arri Priimagi*[a]

Received 30th May 2025,
Accepted 31st July 2025

DOI: 10.1039/d5sm00563a

rsc.li/soft-matter-journal

Reproducing cell–cell and cell–extracellular matrix (ECM) interactions remains a challenge when developing new biomaterials. Especially, the dynamic nature of the ECM is often neglected when cells are cultured *in vitro*. Light-responsive materials are promising candidates to mimic the natural behavior of the ECM. However, their long-term stability under cell culture conditions has not been widely studied. Here, we explore the impact of thin poly(dimethylsiloxane) (PDMS) and poly(*para*-chloroxylylene) (parylene C) coatings on the stability and biocompatibility of azobenzene-based films that can be photopatterned in response to laser interference irradiation. We study the effect of the polymer coatings on the formation, erasure, and reconfiguration of surface relief gratings (SRGs) in dry and aqueous environments. Our results show that parylene C provides significant advantages over PDMS coatings, including improved stability, biocompatibility, and cell adhesion, opening new possibilities for cell-culture-compatible azobenzene-based materials in biomedical applications.

1. Introduction

When culturing cells *in vitro*, it is difficult to mimic the dynamic nature of the cellular *in vivo* microenvironment and its effect on the physiology of the cells.[1] Cells perceive mechanical signals using mechanosensitive molecules and proteins which convert these signals into biochemical activity in a process called mechanotransduction.[2,3] Different mechanical signals originating from the extracellular matrix (ECM) and neighboring cells affect the biological functions of cells, such as growth, migration, and differentation.[4–6] Thus, appropriate cell–material interface composition and its dynamic control are vital to mimic the native cell–ECM interactions. This demands for cell culture substrates with good mechanical, chemical, and topographical properties.[7]

Smart stimuli-responsive biomaterials capable of responding to different external stimuli offer new ways to dynamically modify the material properties and study the cell responses spatiotemporarly.[8–11] Light is a promising stimulus for smart cell-instructive materials since the properties of light can be precisely controlled and localized to a specific target.[12–15] Arguably, the most studied molecules for light-responsive smart materials are azobenzene derivatives. They undergo photoisomerization between stable *trans* and metastable *cis* isomers when illuminated with specific wavelengths.[16,17] Azobenzenes can be incorporated into *e.g.* polymers, liquid crystals, and hydrogels, enabling reversible photocontrol of chemical, mechanical and optical properties. These materials have shown promise as dynamic cell culture platforms able to guide cell morphology, alignment, and adhesion.[18–27] Thin films of azobenzene-based materials can be photopatterned when exposed to laser interference irradiation, to yield macroscopic surface relief gratings (SRGs) on the material surface.[28,29] The formed topographic patterns are reversible and can be erased thermally or optically.[30–32] SRGs have been used as dynamic cell culture substrates to control the alignment and growth of, for example, neurons, fibroblasts and endothelial cells.[19,33–36] As previously reported, epithelial cell alignment and migration can be controlled with SRGs inscribed on a surface of a Disperse Red 1-based amorphous molecular glass (DR1g).[37,38] Inscription and erasure of different surface features has been done during live cell culture using a laser scanning confocal microscope.[36,39,40]

Azobenzene-containing thin films have limitations in terms of stability in an aqueous environment. For example, formation of blister-like structures at the interface between the DR1g film and the glass substrate is observed when the film is immersed in water.[36,41] This occurs when water molecules penetrate through the hydrophobic film towards more hydrophilic substrates, causing local delamination of the film. Another potential problem is the partial dissolution of some azobenzene-based films in the aqueous environment.[42] These issues compromise film

[a] *Faculty of Engineering and Natural Sciences, Tampere University, Tampere, Finland. E-mail: chiara.fedele@tuni.fi, arri.priimagi@tuni.fi*
[b] *Faculty of Medicine and Health Technology, Tampere University, Tampere, Finland*

integrity and functionality over time limiting their use in long-term cell culture applications. Materials used as cell culture substrates should be non-toxic, stable under aqueous conditions to enable light-induced movements, and responsive to cell-safe wavelengths. Modular materials, in which the polymer backbone is fixed and the light responsive units can be changed at will to offer extended sensitivity to light, could be key to obtaining a library of light-responsive, biocompatible materials for multiple purposes. Supramolecular chemistry has enabled the design of such modular biomaterials; however, achieving all required properties simultaneously can be a complex task.[43,44]

To overcome these problems, surface functionalization and protective coatings have been studied to improve the stability of azobenzene-based materials in the cell culture environment.[38,42,45] Especially, polymer coatings can enhance the biocompatibility and functionality of material surfaces.[46–48] Poly(dimethylsiloxane) (PDMS) and poly(*para*-chloroxylylene) (parylene C) are polymers which have excellent properties (*i.e.* biocompatible, chemically inert, optically transparent, and easily fabricated) for biomedical applications.[49,50] Both polymers have been widely used as cell culture substrates and coating materials.[51–63] In addition, parylene C is FDA-approved, making it a desirable material for biological applications, such as neural prostheses, blood contacting implants and implantable electronic devices.[64–68] It has been previously shown that PDMS coating allows independent control of mechanical and chemical cues when deposited on a DR1g film.[38] Although the PDMS coating improves the material stability, it does not prevent the aforementioned blister formation completely. Compared to PDMS, parylene C has lower water permeability and higher solvent compatibility and is mechanically robust. These properties are associated with the dense crystalline structure, which is why parylene C is an excellent material for barrier applications.[69,70]

Here, we compare PDMS and parylene C coatings for improving the stability and biocompatibility of azobenzene-based thin films in an aqueous environment. Our goal is to develop a polymer coating that acts as a protective layer, preventing blister formation and dissolution while allowing the inscription of light-induced topographic patterns. Both coatings fulfil the latter goal; but compared to PDMS, parylene C offers improved stability of the azobenzene films against both blister formation and dissolution. Parylene C also improves biocompatibility and cell adhesion during cell culture experiments with epithelial cells. Our results demonstrate that parylene C coating provides an effective barrier and improves the stability of azobenzene-based materials in an aqueous environment, which opens possibilities to use a wider variety of light-responsive materials for cell culture applications.

2. Results and discussion

2.1. SRG formation and erasure under dry conditions

In this study, we used DR1g as a light-responsive substrate unless otherwise specified. DR1g is a commercially available photoresponsive molecular glass, consisting of a mexylaminotriazine precursor (glass-forming component) and a Disperse Red 1 (DR1, light-responsive component) dye (Fig. 1a).[30] The molecular structure of mexylaminotriazines can be easily tuned

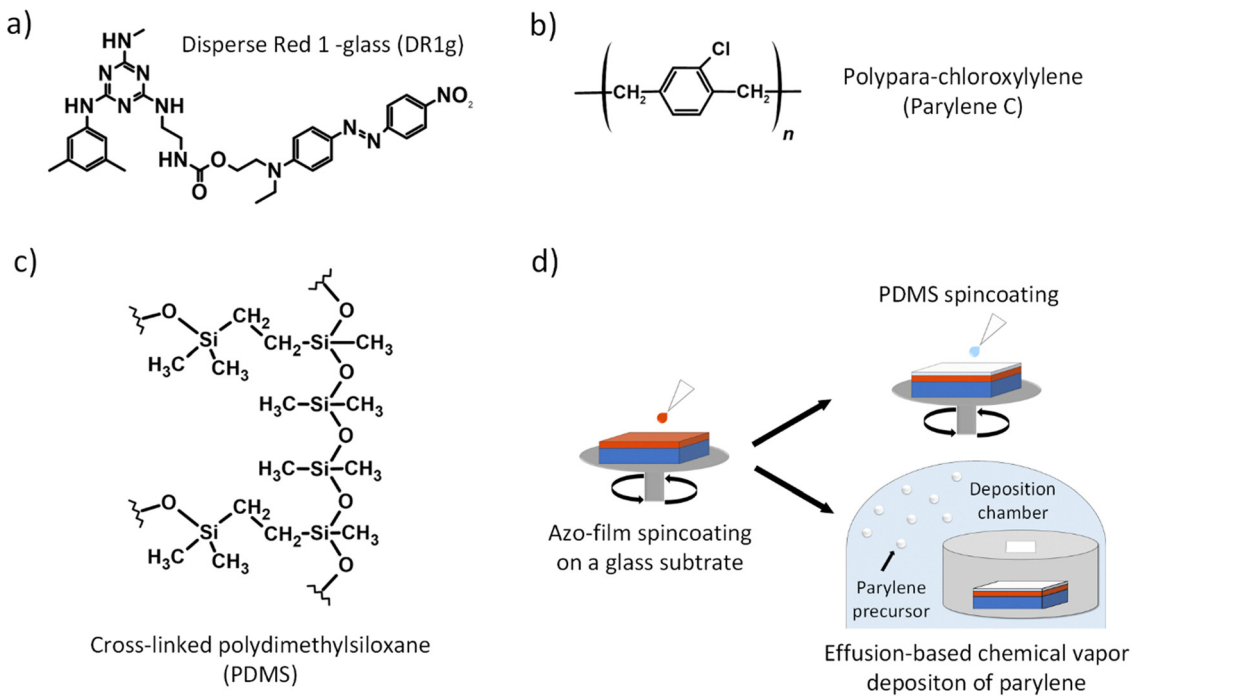

Fig. 1 Chemical structures of (a) light-responsive DR1g, (b) parylene C and (c) cross-linked PDMS. (d) Schematic illustration of the sample fabrication process. First, azobenzene-based thin films are spin coated on a glass substrate. Subsequently, the PDMS coating is fabricated by spin coating and the parylene C coating is fabricated by effusion-based CVD.

and they can be incorporated into other moieties to promote glass-forming ability and prevent crystallization of the film.[71] The DR1 chromophore has shown efficient SRG formation and its photochemical properties have been widely studied.[72] Compared to DR1 polymer counterparts (*e.g.* poly-disperse red 1-methacrylate), DR1g offers improved glass-forming ability and more reproducible material properties, and it can be easily fabricated into high quality thin films. The glass-forming moiety does not hinder the optical properties of DR1, and DR1g has shown excellent SRG formation. Due to these properties, DR1g is an appealing material for light-responsive cell culture substrates.

Thin DR1g films were fabricated *via* spin coating (thickness of 270 ± 20 nm) and subsequently coated with parylene C (Fig. 1b) or PDMS (Fig. 1c). Fig. 1d shows schematic illustration of the sample fabrication process. The PDMS coatings (65 ± 10 nm) were obtained using spin coating as previously reported.[38] Parylene C films are generally prepared *via* chemical vapor deposition (CVD), during which a solid parylene C dimer is vaporized, pyrolyzed into reactive monomers at high temperature in a furnace, and polymerized in a deposition chamber to form a conformal coating.[50,73] To achieve films with thicknesses below 100 nm, we used the effusion-based CVD method described by Liu *et al.* to produce uniform parylene C films with a thickness of 55 ± 10 nm (Fig. S1).[74] Parylene C-coated and PDMS-coated DR1g films were denoted as $DR1g_{ParC}$ and $DR1g_{PDMS}$, respectively.

SRGs with 1 μm periodicity were inscribed on the DR1g surface using interference lithography in Lloyd's mirror configuration (488 nm, circular polarized light, 500 mW cm^{-2}).[28] The inscription (and erasure) was monitored by recording the first-order diffracted signal of a 633 nm laser (Fig. 2a; see Materials and Methods for further experimental details). $DR1g_{ParC}$ samples consistently exhibited higher diffraction efficiency (DE) (18 ± 3%, n = 3) compared to non-coated DR1g films (14 ± 1%, n = 3). The higher standard deviation for $DR1g_{ParC}$ is likely due to small variations in the parylene C coating thickness. $DR1g_{PDMS}$ films reached DE comparable to the non-coated films (13 ± 1%, n = 3, Fig. S2a), in accordance with previous observations.[38] With longer inscription time (>30 min, Fig. S3), the DE for DR1g samples reached approximately 20 ± 1%, similar to that for $DR1g_{ParC}$.

The shape and height of the SRGs were characterized using atomic force microscopy (AFM; Fig. 2b, e and Fig. S2c and d), revealing modulation depths of 370 ± 25 nm for $DR1g_{ParC}$, 315 ± 10 nm for $DR1g_{PDMS}$, and 275 ± 15 nm for non-coated DR1g films. Both polymer-coated films exhibited higher SRG amplitudes compared to non-coated DR1g films, possibly due to polymer accumulation on the SRG peaks. Thicker parylene C coatings (>100 nm) delayed the SRG formation (Fig. S1b), while thinner coatings (~55 nm) did not. This is consistent with earlier reports on plasma-polymerized acrylic acid coatings.[42] Despite parylene C's relatively high Young's modulus (2.8 GPa) in the bulk, it seems to enhance the SRG formation, unlike the softer PDMS (1.2 MPa) or uncoated DR1g (580 MPa as measured *via* nanoindentation).[64,75] It is known that in thin polymer coatings

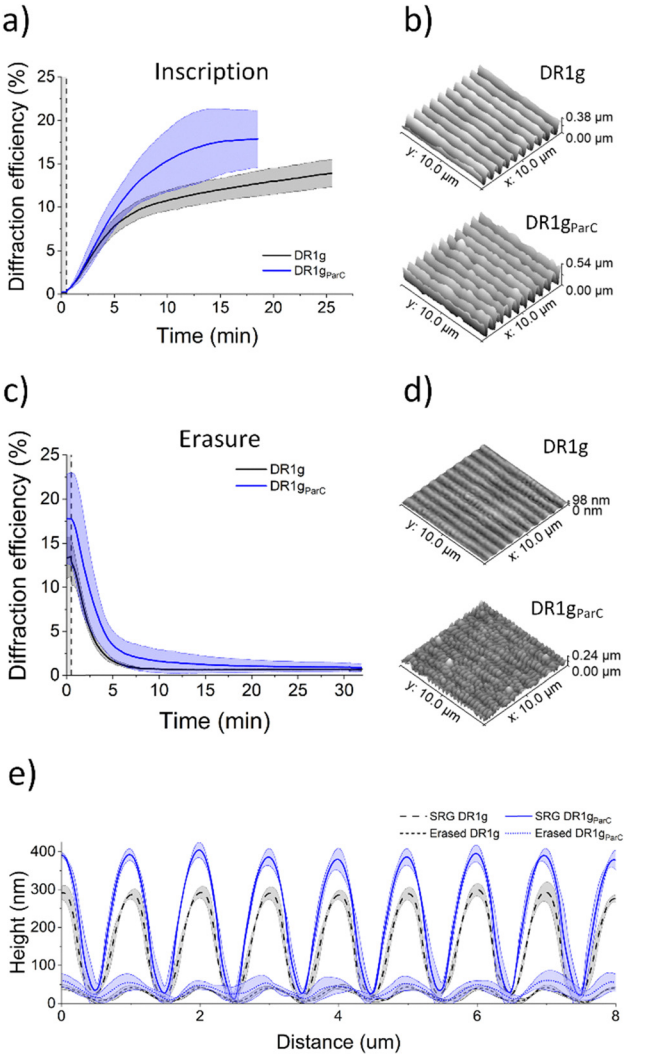

Fig. 2 (a) Diffraction efficiency (DE) measured during SRG inscription (488 nm, 500 mW cm^{-2}) and (b) corresponding AFM images of the inscribed SRG topographies on non-coated DR1g and $DR1g_{ParC}$ films. (c) DE measured during SRG erasure (488 nm, 500 mW cm^{-2}) and (d) corresponding AFM images of the erased surface. (e) 1D surface profiles of SRG and erased topographies for non-coated DR1g and $DR1g_{ParC}$ films. The thick lines in the DE and surface profile graphs present the average value, and the lighter colored area represents the standard deviation over three independent measurements.

the mechanical properties may deviate from bulk ones due to the nanoconfinement of polymer chains.[76] For instance, the Young's modulus of PDMS has been reported to increase with decreasing thickness.[77] AFM nanoindentation measurements revealed that the thin $DR1g_{ParC}$ film exhibits a similar Young's modulus (2.4 GPa) to that of the bulk material. However, flexural rigidity (materials ability to resist bending) is sensitive to thickness changes and it decreases in proportion to the cube of the film thickness.[78,79] This is why thin films made of materials typically regarded as stiff can still be flexible. In addition, SRG inscription subjects the polymer coating to complex force fields, which differ from the uniaxial stress in standard tensile testing, complicating the actual response of such multilayered materials even further.

The inscribed SRGs can be erased with a uniform circularly polarized laser beam. The parylene C and PDMS coatings did not hinder the erasure process, as shown in Fig. 2c and Fig. S2b. The rate of erasure was almost equal for DR1g and $DR1g_{ParC}$ films, as confirmed by comparing the curve slopes of the erasure, k, at the steepest regime ($k = -0.07$ for DR1g and $DR1g_{ParC}$). In line with previous observations, the PDMS coating accelerates the SRG erasure ($k = -0.15$ for $DR1g_{PDMS}$).[38] Despite the vanishing of the diffracted signal, small remnant SRGs with modulation depths of 45 ± 15 nm ($DR1g_{ParC}$), 50 ± 20 nm ($DR1g_{PDMS}$) and 35 ± 10 nm (non-coated DR1g) were observed on all films (Fig. 2d, e and Fig. S2c, d). $DR1g_{PDMS}$ and $DR1g_{ParC}$ also showed secondary grating structures, resembling spontaneous surface topographies reported on

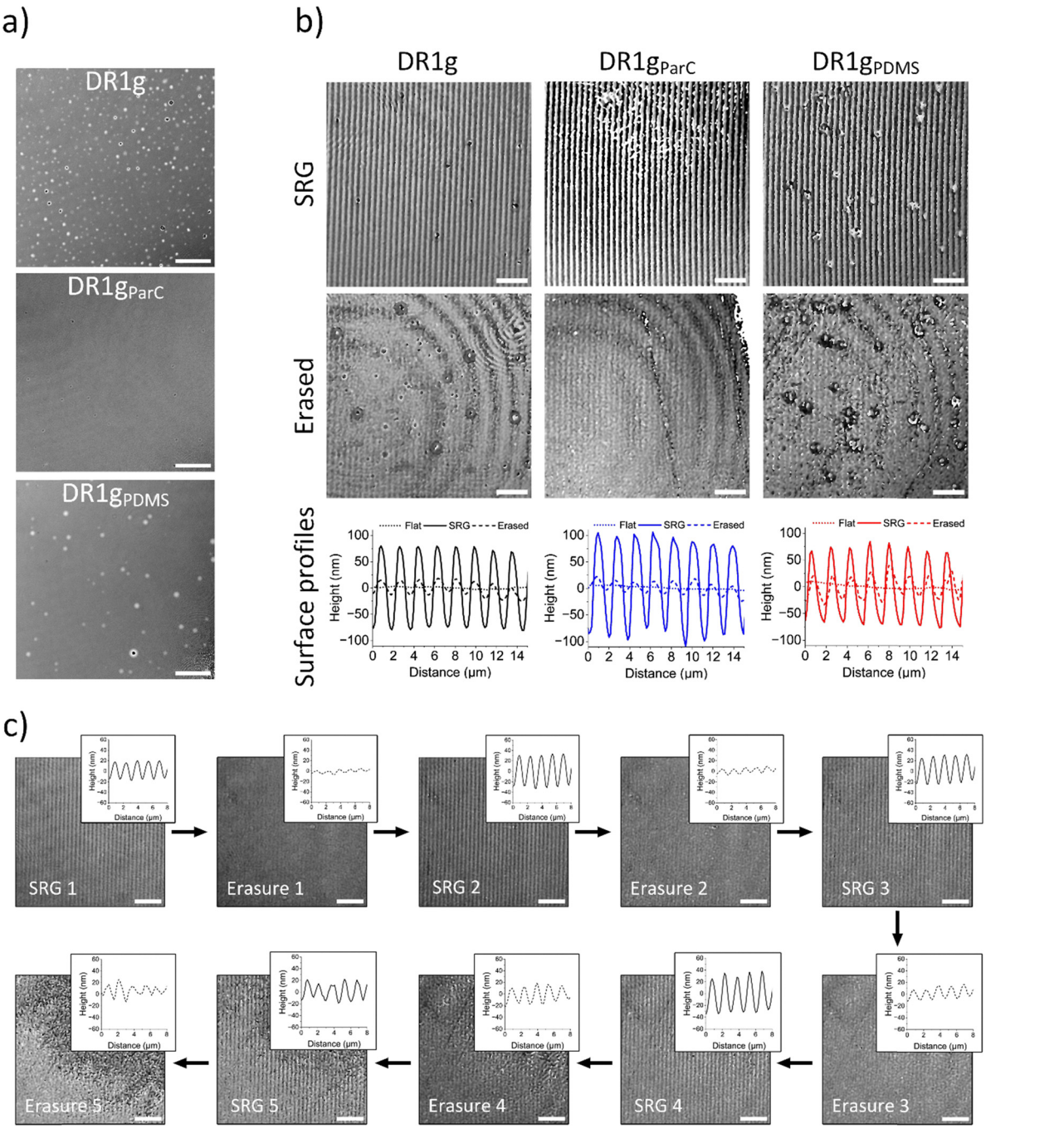

Fig. 3 (a) Surface of DR1g, $DR1g_{ParC}$ and $DR1g_{PDMS}$ films after immersion in water. Blisters can be seen forming on non-coated DR1g films and $DR1g_{PDMS}$ films but not on $DR1g_{ParC}$ films. Images are taken with DHM with a scale bar of 20 μm. (b) DHM images of inscribed and erased SRG topography in water for non-coated DR1g, $DR1g_{ParC}$ and $DR1g_{PDMS}$. Surface profiles show the flat surface at the beginning and the SRG height after inscription and erasure. The scale bar is 20 μm. (c) DHM images and surface profiles of the inscribed and erased SRG topographies during multiple inscription/erasure cycles in the aqueous environment for $DR1g_{ParC}$ films. The scale bar is 10 μm.

azobenzene-based films.[80–82] This can be due to plastic deformation of the polymer coatings during the erasure process. Similar wavy patterns have been reported on parylene C-coated elastomer substrates when the film is first stretched and then compressed.[83]

2.2. SRG formation and erasure in the aqueous environment

A key requirement for dynamic, reconfigurable cell-instructive surfaces is achieving multiple inscription–erasure cycles in the aqueous environment. Rianna *et al.* previously demonstrated rewriting of the surface patterns with live cells, but the topography was erased and rewritten only after removal of the cell culture medium.[39] A drawback of DR1g in the aqueous environment is the formation of blister-like structures, caused by local film delamination. Mauro *et al.* have shown that silane functionalization stabilizes the glass–azopolymer interface, enabling dynamic modulation of the azopolymer surface in the presence of aqueous solution.[45] Here, the effect of polymer coatings during inscription–erasure cycles in water was investigated using a digital holographic microscope (DHM) equipped with a custom-built interference lithography system, enabling real-time monitoring of surface topography across multiple cycles.[84,85]

Blisters appeared on non-coated DR1g and DR1g$_{PDMS}$ samples but were largely absent on DR1g$_{ParC}$ as shown in Fig. 3a. The difference between PDMS and parylene C coatings most likely stems from their distinct material properties. PDMS is a soft, porous elastomer, whereas parylene C is semicrystalline and has higher Young's modulus, resulting in significantly lower water permeability.[50,86] Also, the fabrication methods differ: PDMS is applied *via* spin coating, which is user-dependent and prone to surface defects, whereas parylene C is deposited through vacuum CVD, yielding uniform, conformal, and defect-free coatings. Since blistering tends to occur around surface defects, the higher defect density in PDMS-coated films likely promotes blister formation.[41]

SRGs could be inscribed and erased efficiently in water, yet blistering occurred on non-coated DR1g and DR1g$_{PDMS}$ films (Fig. 3b). On DR1g$_{ParC}$, no blisters were formed even during inscription and erasure. The process was cycled five times for DR1g and DR1g$_{ParC}$ films (Fig. 3c and Fig. S4). For DR1g$_{ParC}$, the SRG height decreased after four cycles, though remaining visible even after the fifth cycle. However, erasure efficiency dropped already during the third cycle. In comparison, non-coated DR1g films showed no notable degradation across cycles. We attribute the reduced performance of DR1g$_{ParC}$ to partial delamination of the parylene C layer, likely due to mechanical fatigue and weakened adhesion to the DR1g film, hindering topography transfer from the photoresponsive film to the passive coating.[87] Parylene C's low adhesion is a known limitation for example in MEMS systems.[63] Various strategies, including high-temperature annealing, have been proposed to improve parylene C adhesion, and will be the subject for further study.[88–91]

2.3. Barrier properties of the polymer coatings in aqueous environment

To further study the barrier properties of the coatings, their ability to protect an underneath light-responsive material that is unstable in the aqueous environment was tested. Supramolecular materials have been used to design modular materials, whose properties can be tuned for specific purposes.[44] Using the same backbone polymer, the optical properties can be changed using different chromophore sidechains. With modular design, a library of different azobenzene-based materials for cell culture studies could be made. However, supramolecular side-chain polymers, including light-responsive ones, are more prone to phase separate, crystallize, or dissolve in the aqueous environment. To expand the range of cell culture-compatible light-responsive materials, protective polymer coatings may offer a particularly promising strategy.

To test this, a thin film (310 ± 20 nm) of hydrogen-bonded supramolecular complex consisting of a poly(4-vinyl pyridine) (P4VP) backbone and a 4-hydroxy-4′-dimethylaminoazobenzene (OH-DMA) chromophore was used as the substrate.[92,93] The complex is referred here as P4VP(OH-DMA) and its structure is

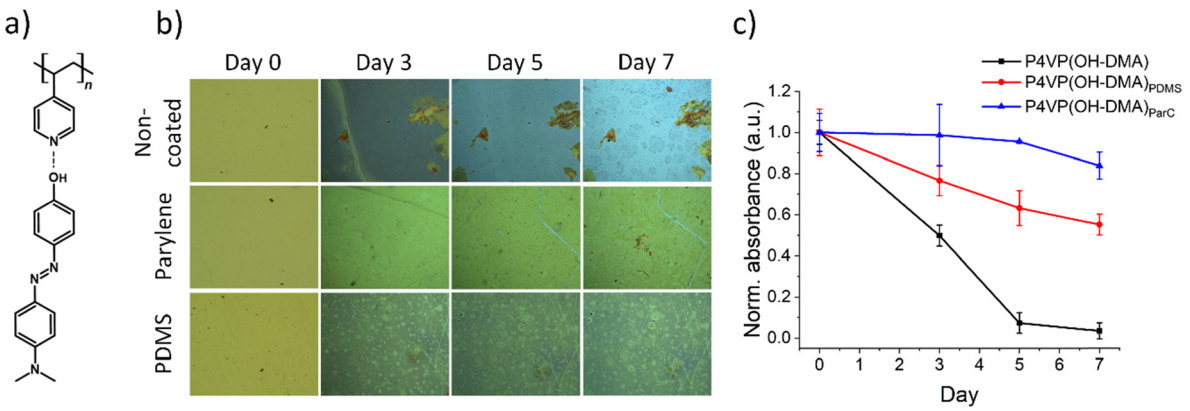

Fig. 4 (a) Chemical structure of P4VP(OH-DMA). (b) Optical micrographs of P4VP(OH-DMA) (top), P4VP(OH-DMA)$_{ParC}$ (middle) and P4VP(OH-DMA)$_{PDMS}$ (bottom) films before, after 3 days, 5 days and 7 days of incubation in a cell medium droplet. (c) Absorbance of P4VP(OH-DMA) at 415 nm for P4VP(OH-DMA), P4VP(OH-DMA)$_{PDMS}$ and P4VP(OH-DMA)$_{ParC}$ during the 7-day incubation in the cell medium droplet. Error bars present the standard deviation over two measurements.

shown in Fig. 4a. The optical properties of P4VP(OH-DMA) can be controlled by changing the molecular weight of P4VP and the complexation degree (the number of chromophores per repeating polymer unit). This material exhibits efficient SRG formation, but is not suitable as cell culture substrates due to the hydrophilic nature of P4VP, making the films unstable in the aqueous environment (Fig. S5).[94] Non-coated P4VP(OH-DMA) and coated P4VP(OH-DMA)$_{ParC}$ and P4VP(OH-DMA)$_{PDMS}$ were tested by placing a droplet of cell culture medium on their surface and incubating at 37 °C in a humidified atmosphere with 5% CO_2. Film stability was monitored over seven days using optical microscopy and UV-vis spectroscopy.

The microscopy images (Fig. 4b) show that the P4VP(OH-DMA) film detached from the substrate during the 7-day incubation. The P4VP(OH-DMA)$_{PDMS}$ film also degraded, as evident from color fading. In contrast, no significant color fading was observed for P4VP(OH-DMA)$_{ParC}$, indicating more effective protection. Absorbance measurements (Fig. 4c) confirmed this observation: for the uncoated film, the absorbance of OH-DMA vanished by day five, while the P4VP(OH-DMA)$_{PDMS}$ film showed a gradual absorbance decline. Both also exhibited the broadened and red-shifted OH-DMA absorption band (Fig. S6), suggesting molecular aggregation or phase separation. The P4VP(OH-DMA)$_{ParC}$ film largely retained its absorbance and spectral shape, confirming improved barrier performance. This difference can be attributed to lower gas (O_2) and water permeability of parylene (2.8 cm^3 mm m^{-2} day atm and 1.68 g mm m^{-2} day) compared to PDMS (52 000 cm^3 mm m^{-2} day atm and 125 g mm m^{-2} day), highlighting its suitability as a protective coating as thin as 50 nm.[95,96] However, ultrathin parylene coatings may contain occasional pinholes, which likely account for the slight absorbance decrease after five days of incubation due to minor liquid penetration.[97] In addition, soaking parylene C films in liquid for extended periods may lead to water vapor infiltration.[90] Importantly, the protection is effective for time scales relevant for cell culturing, ensuring the durability and reliability needed for dynamic surface patterning in biological applications.

2.4. Biocompatibility of polymer-coated DR1g and P4VP(OH-DMA) films

The polymer coating is also aimed at improving material biocompatibility in cell culture studies. Both formation of blisters on DR1g and dissolution of P4VP(OH-DMA) in the aqueous environment can negatively affect the cell growth. We hypothesized that P4VP(OH-DMA), due to its poor stability, would not be a suitable substrate for cell culture studies. In contrast, DR1g films have not shown cytotoxic effects in short-term cell culture studies, but the long-term biocompatibility has not been widely analyzed. Here, we applied epithelial Madin-Darby canine kidney type II (MDCK II) cells, which were seeded on collagen I-coated P4VP(OH-DMA), P4VP(OH-DMA)$_{PDMS}$, P4VP(OH-DMA)$_{ParC}$, DR1g, DR1g$_{PDMS}$, and DR1g$_{ParC}$ films and cultured for seven days. The collagen coating was used to improve cell adhesion of epithelial cells on the material surface.[37] Microscopy imaging and immunostaining were used to investigate the effects of PDMS and parylene C coatings on the cellular behavior by observing epithelial cell growth and monolayer formation as well as the surface adhesion and monolayer maturation.

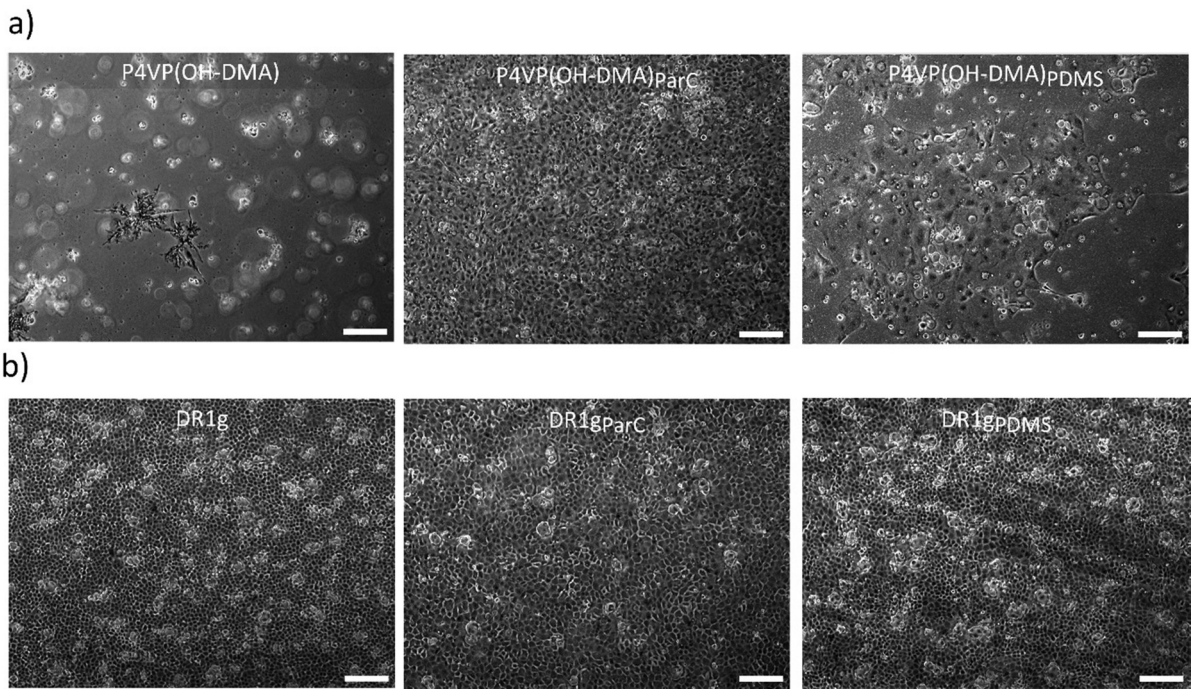

Fig. 5 Light microscopy images of Madin-Darby canine kidney type II (MDCK II) epithelial cells cultured on (a) P4VP(OH-DMA), P4VP(OH-DMA)$_{ParC}$ and P4VP(OH-DMA)$_{PDMS}$ films, and (b) DR1g, DR1g$_{ParC}$ and DR1g$_{PDMS}$ films for seven days. The scale bar is 200 μm.

Cell debris and non-attached cells were observed on non-coated P4VP(OH-DMA) after seven days of culture, indicating cytotoxicity or poor biocompatibility (Fig. 5a). In contrast, P4VP(OH-DMA)$_{ParC}$ films supported uniform monolayer formation. On P4VP(OH-DMA)$_{PDMS}$ films, some attached and dividing cells were observed, but the films lacked a uniform epithelium layer, indicating reduced cell attachment or proliferation. These findings suggest that polymer coatings improve the biocompatibility of P4VP(OH-DMA), with parylene C offering improved support for cell growth and monolayer formation compared to PDMS. On DR1g films, all samples supported epithelium formation by day seven, with no visible differences (Fig. 5b). The presence of cellular domes, a sign of mature epithelium, further confirmed epithelial integrity.[98–100] Thus, the long-term cell growth was continued with weekly monitoring. A previous work of Ristola *et al.* demonstrated culturing of neuronal cells on DR1g films for up to six weeks, prompting us to extend the culture period to 10 weeks.[35] During this period, small holes were observed in the cell monolayer on DR1g$_{PDMS}$ films after four weeks, indicating localized cell detachment (Fig. S7a). Floating cells were also observed on the well surface of non-coated DR1g films by week seven (Fig. S7b). In contrast, DR1g$_{ParC}$ films maintained a uniform, tight epithelium layer throughout the 10-week culturing period.

Immunostaining and confocal imaging were used to evaluate epithelial cell adhesion and growth on the different substrates. Epithelial integrity and attachment were assessed with phosphorylated focal adhesion kinase (pFAK)-associated focal adhesions and strong zonula occludens 1 (ZO-1)-associated tight junctions, while DAPI staining was used to detect nuclei and distinguish individual cells.[3,101–103] On non-coated P4VP(OH-DMA) films, cells were poorly attached and mostly dead, with only few deformed cells found attached to the surface (Fig. 6a). Cells cultured on P4VP(OH-DMA)$_{ParC}$ and P4VP(OH-DMA)$_{PDMS}$ formed mature epithelia, with ZO-1 localized between the cell–cell contacts and pFAK strongly expressed on the basal side of the cells (Fig. 6a). Parylene C-coated substrates supported epithelial cells with typical polygonal morphology, while PDMS-coated films showed variable, deformed cell shapes, differing from the normal morphology seen on control glass (Fig. S8a). These observations align with the one-week incubation results (Fig. 4). The dissolution of P4VP(OH-DMA) in non-coated and PDMS-coated films likely contributed to cytotoxicity and poor cell viability. In contrast, parylene C coatings minimized dissolution, supporting

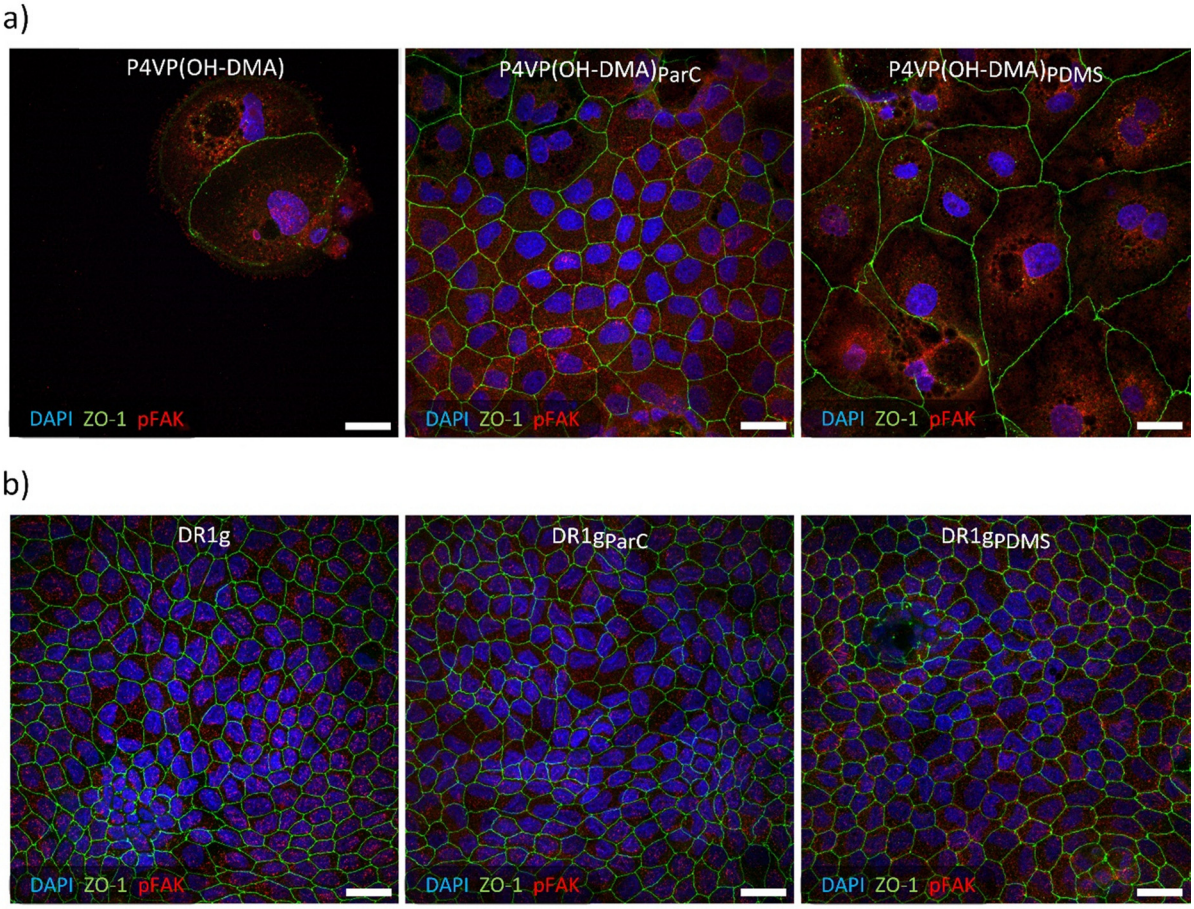

Fig. 6 (a) MDCK II epithelial cells seeded on P4VP(OH-DMA), P4VP(OH-DMA)$_{PDMS}$ and P4VP(OH-DMA)$_{ParC}$ samples and cultured for seven days. (b) MDCK II epithelial cells seeded on DR1g, DR1g$_{PDMS}$ and DR1g$_{ParC}$ samples and cultured for 10 weeks. Labels used were chromatin (DAPI, blue), tight junctions (ZO-1, green) and mature focal adhesions (pFAK, red). The scale bar is 20 μm.

healthy cell growth and underscoring its protective and biocompatible properties.

Immunostained DR1g samples showed no significant differences in monolayer formation between the substrates (Fig. 6b). ZO-1 localization at cell–cell contacts and basal pFAK expression indicated the formation of tight, intact epithelium and strong cell adhesion. Non-coated DR1g films exhibited no cytotoxic effects, suggesting good stability under extended cell culture conditions. However, $DR1g_{PDMS}$ films displayed cell-free holes in the epithelium, surrounded by enlarged cells (Fig. S8b). Although cells initially grew uniformly across the surface, they later began avoiding these regions and formed multilayers instead. These defects may result from hydrophobic recovery of PDMS or the unsuccessfully bound protein matrix, both of which can impair cell adhesion and promote aggregation.[53,104,105] Strategies like oxygen plasma, ozone treatment, and chemical surface modification may help in preventing this.[106–108] In contrast, parylene C showed no such limitations, making it more suitable for longer culture periods.

3. Conclusions

This study investigated the protective and biocompatible properties of PDMS and parylene C coatings on light-responsive thin films. Both coatings maintained the ability of the DR1g layer to form and erase SRGs. Parylene C effectively prevented blistering of DR1g films in water, unlike PDMS, which offered only partial protection. This feature is critical for enabling controlled cell alignment on dynamic topographies. Reversible SRG inscription and erasure ability was maintained under aqueous conditions. However, partial delamination of parylene C limited repeated inscription–erasure cycles to five.

Parylene C stabilized supramolecular P4VP(OH-DMA) films under water, highlighting its excellent barrier properties and enabling broader material use in cell culture. It also enhanced biocompatibility of P4VP(OH-DMA) and supported uniform, mature epithelial layers even after seven days of culturing. Cell culturing periods of up to 10 weeks were obtained with parylene C-coated DR1g films, while PDMS coatings experienced hydrophobic recovery over time, compromising long-term cell cultures. Overall, parylene C turned out superior for stabilizing azobenzene films and supporting cell culture. Its FDA-approved biocompatibility and ability to withstand aqueous environments make it ideal for advanced, dynamic *in vitro* platforms. Future work should aim to improve SRG reconfigurability and to further explore the parylene C's role in dynamic topographical changes during cell growth.

4. Materials and methods

4.1. Preparation of Disperse Red 1 glass thin films

Thin films of azobenzene-based Disperse Red 1 molecular glass (DR1g, Solaris Chem Inc.) were prepared according to the protocol described in Bachelor thesis by Lotta Kääriäinen.[109] Shortly, 6 wt% solution of DR1g was prepared in a mixture containing a chloroform–1,2-dichloroethane mixture with a ratio of 80 : 20 (v/v). Solution was ultrasonicated and filtered to improve material dissolution, after which it was spin-coated (Laurell Technologies Corporation) on cleaned glass 22 × 22 mm^2 coverslips. Solvents were left to evaporate in a vacuum chamber at 65 °C for 1 h.

4.2. Preparation of azobenzene-based supramolecular thin films

Azobenzene-based supramolecular (P4VP(OH-DMA)) films were prepared by spin coating (Laurell Technologies Corporation). 4-Hydroxy-4′-dimethylaminoazobenzene (OH-DMA, TCI Chemicals) and poly 4-vinyl pyridine (P4VP, M_w: 1200, Polymer Source Inc.) were mixed in a 1 : 3 molar ratio, with one part azobenzene to three parts pyridine. 5 wt% solution was prepared by dissolving the solid components in tetrahydrofuran (THF). 35 μL of the solution was spin coated on cleaned 22 × 22 mm^2 glass coverslips at 3000 rpm for 35 s.

4.3. PDMS deposition

Polydimethylsiloxane (PDMS, SYLGARD 184 Silicone Elastomer, Dow) thin films were fabricated using the same protocol described by Isomäki *et al.* Shortly, 1 wt% PDMS solution was prepared by mixing a polymer elastomer base and a curing agent in a 10 : 1 ratio (w/w) and diluting the uncured PDMS in *n*-hexane. 50 μL of the solution was spin-coated on the top of the DR1g film (or P4VP(OH-DMA) film) at 6000 rpm for 150 s. PDMS films were cured at 55 °C for 1 h.

4.4. Parylene C deposition and thickness measurements

Effusion based chemical vapor deposition of parylene C was used to coat DR1g and P4VP(OH-DMA) films. Here, the samples were placed inside secondary deposition chambers with 1000 μm square holes on the lids to control the pressure of the deposition and therefore the thickness of the prepared parylene C films. More detailed description of the optimization process can be found in the SI. Parylene deposition machines (Para Tech Coating Inc. and SCS Labcoater 2) were used for the coating process. The secondary chambers were placed inside the principal machine deposition chamber and the powder type dichloro-*p*-cyclophane dimer (Galentis Ltd) was loaded into the deposition serving system. The final thickness of the films was measured with a stylus profilometer (Veeco Dektak 150). All measured thickness values are presented as mean ± SD.

4.5. Surface relief grating inscription and erasure under dry conditions

Inscription of surface relief gratings (SRGs) (1 μm microtopography period) on DR1g films was done using Lloyd's mirror configuration and a 488 nm continuous-wave laser (Coherent Genesis CX488-2000) with circular polarization and an intensity of 500 mW cm^{-2}. More detail description of the set-up is described by Isomäki *et al.*[28] For SRG erasure, samples were removed from Lloyd's mirror configuration and placed perpendicular to the laser beam to get a uniform laser beam. An intensity of 500 mW cm^{-2} was used. A low-power (1 mW) 633 nm He–Ne laser was used to monitor the inscription and

erasure process, during which the power of the first order diffracted beam was measured. Diffraction efficiency (DE) was calculated by dividing the power of the first order diffracted beam with the incident power of the probe beam. The rate of the erasure process was calculated from the slope of the line formed at the steepest point of the curve. The equation of the slope was calculated with OriginLab software.

4.6. SRG characterization with AFM

AFM images were acquired with a Bruker Dimension Icon atomic force microscope in the Peak Force Tapping mode. Silicon nitride ScanAsyst-Air probes (Bruker) were used in the imaging (nominal spring constant: 0.4 N m^{-1}). The imaging area was 10 μm by 10 μm, the resolution was 512 by 512 pixels, and the scan rate was from 0.1 Hz to 0.3 Hz depending on the sample. The scan direction was perpendicular to the direction of the grating. Captured images were analyzed using Gwyddion (2.65) software. All measured topography heights are presented as mean ± SD.

4.7. Mechanical characterization with AFM

The Young's moduli of the DR1g sample and polymer coatings were measured using AFM Peak Force Quantitative Nanomechanical Mapping (PF-QNM) with a ScanAsyst AIR silicon tip on nitride lever (Bruker). Deflection sensitivity was calibrated using fused silica as a reference sample (FSILICA-12M). The average value from three force curves was calculated as 34.25 nm V^{-1}. The tip radius was measured using a titanium reference sample (RS-12M). The Young's modulus was then measured as the area average using Nanoscope software (Bruker).

4.8. Surface topography inscription and erasure in the aqueous environment

A digital holographic microscope (DHM R-2100, LyncéeTec) was used to monitor the surface topography formation and erasure in an aqueous environment. A custom integrated interference lithography system coupled to the DHM was used to inscribe and erase SRGs on sample surfaces multiple times in a row. The detailed description of the setup was provided by Rekola *et al.*[72] Samples were immersed in deionized water and irradiated with the laser (Coherent Genesis CX-488 2000) coupled to the DHM. Circularly polarized light with a 488 nm wavelength and a 5.90 W cm^{-2} intensity was used to create a sinusoidal interference pattern with 1 μm periodicity. A 40× water-immersion objective (0.8 NA, Olympus LUMPLFLN40XW) was used for imaging. The erasure of the topography was done by blocking one of the laser beams to create a uniform light beam with 2.95 W cm^{-2} intensity.

4.9. Stability of the polymer-coated azobenzene-based supramolecular films

Non-coated and polymer-coated P4VP(OH-DMA) films were sterilized under UV for 30 min. 200 μL drops of MEM without Phenol red (Gibco) were inserted on top of the samples and the samples were incubated at 37 °C, under a humidified atmosphere with 5% CO_2. After 24 h of incubation, the drops were aspirated and the samples were fully dried. Absorbances were measured between 180 and 1100 nm wavelengths with a UV/vis spectrophotometer (Ocean Optics DH-2000-BAL deuterium and tungsten halogen lamp combination as a light source and Avantes Starline AvaSpec-2048L as a photodetector). A polarized optical microscope (Zeiss Axio Scope. A1, NAchroplan air-immersion 5×/0.13 Pol ∞/0 objective) was used to image sample surfaces. After measurements, new drops of MEM were inserted, and the samples were moved back to the incubator (37 °C, 5% CO_2). Removal of the drops, absorbance measurements and optical imaging as well as insertion of new drops followed by incubation were repeated daily for 7 days. Absorbance curves were analyzed with OriginLab (version 10.0.5.157) and the scattering effect was removed by vertical translation of the curves. The absorbance value was shifted to 0 at the lowest absorbance value between 300 and 800 nm.

4.10. Cell culture

Madin-Darby canine kidney type II wild type epithelial cells (MDCK II) were cultured in MEM GlutaMax (Gibco) supplemented with 10% fetal bovine serum (Gibco) and 1% penicillin/streptomycin (Gibco) at 37 °C under a humidified atmosphere with 5% CO_2. Prior to cell seeding, the samples were treated with oxygen plasma (Pico, Diener electronic GmbH), coated with 0.1 mg mL^{-1} collagen I (Gibco) in 0.02 N acetic acid, and sterilized under UV for 40 min. For testing the protectiveness of the layers, MDCK II cells were cultured on non-coated (n = 4), PDMS-coated (n = 2) and parylene C-coated (n = 4) P4VP(OH-DMA) films. The samples were imaged with a light-microscope (Zeiss Vert. A1 microscope, Zeiss AxioCam MRc5, Zeiss N-ACHROPLAN 5×/0.15 Ph1) and the media was changed after 24 h and 72 h. After 7 d of culture, the samples were fixed and immunostained. For long-term cell culture, MDCK II cells were cultured on non-coated (n = 4), PDMS-coated (n = 4) and parylene C-coated (n = 4) DR1g films. The samples were imaged with a light-microscope (Zeiss Vert. A1 microscope, Zeiss AxioCam MRc5, Zeiss N-ACHROPLAN 5×/0.15 Ph1) after 24 h, 72 h, 1 week and weekly from there on until ten weeks. The MEM was changed weekly by removing the old media, washing the samples with DPBS (Gibco) and adding new media to the samples. After ten weeks, the samples were fixed and immunostained.

4.11. Fixing and immunostaining

Cells were fixed with 4% PFA solution (Electron Microscopy Sciences) for 10 min at RT, washed twice with DPBS (Gibco), permeabilized with permeabilization buffer containing 0.5% bovine serum albumin (BSA, PAN Biotech) and 0.5% Triton-X 100 (Sigma Aldrich) and blocked with 3% BSA in DPBS at RT for 1 h. Labels used were mouse ZO-1 monoclonal antibody (ZO1-1A12) (1 : 50, Invitrogen, #33-9100) and rabbit anti-pFAK (1 : 200, Abcam, #ab81298). The secondary antibodies used were Alexa Fluor™ 488 goat anti-mouse IgG (1 : 200, Invitrogen, #A11029) and Alexa Fluor™ 568 goat anti-rabbit IgG (1 : 200, Invitrogen, #A11011). Nuclei were labeled with 4',6'diamidino-2-phenylindole (DAPI, 1 : 1000). Samples were mounted with a prolong diamond antifade mountant with 4',6'diamidino-2-phenylindole (DAPI) (Invitrogen) and dried covered from light

at room temperature. Confocal imaging (Nikon A1R laser scanning confocal microscope, Nikon Instruments Europe BV) was used to image the immunostained samples with 405 nm, 488 nm, and 568 nm laser lines. The laser intensity and detector sensitivity were adjusted for each image to obtain optimal image brightness and to avoid photobleaching. A 60×/1.4 Plan-Apochromat oil immersion DIC N2 objective was used to capture 1024 × 1024-pixel snapshots and *z*-stack with a 150–250 nm interval. Images were processed with ImageJ software.

Conflicts of interest

The authors declare no conflicts of interests.

Data availability

The data that support the findings of this study are openly available in Zenodo at **https://doi.org/10.5281/zenodo.15995750**.

Data on parylene C coating optimization, PDMS-coated sample characterization, long inscription DE, inscription-erasure cycles of DR1g sample, UV-Vis and supporting cell images) is available. See DOI: **https://doi.org/10.1039/d5sm00563a**.

Acknowledgements

This project was supported by the Instrumentarium Science Foundation and the Research Council of Finland Center of Excellence on Life-Inspired Hybrid Materials Research (LIBER; No. 346107). The authors acknowledge the Biocenter Finland (BF), Tampere Microscopy Center (TMC) and Tampere Imaging Facility (TIF) for their services. This work was conducted as part of Academy of Finland Flagship Programme, Photonics Research and Innovation (PREIN; No. 320165). The authors thank Dr Petri Mustonen for his assistance with parylene C coating, and Matias Paatelainen for his assistance with atomic force microscopy.

References

1 M. W. Tibbitt and K. S. Anseth, *Sci. Transl. Med.*, 2012, **4**, 160ps24.
2 J. Eyckmans, T. Boudou, X. Yu and C. S. Chen, *Dev. Cell*, 2011, **21**, 35–47.
3 F. Martino, A. R. Perestrelo, V. Vinarský, S. Pagliari and G. Forte, *Front. Physiol.*, 2018, **9**, 824.
4 T. Dvir, B. P. Timko, D. S. Kohane and R. Langer, *Nat. Nanotechnol.*, 2011, **6**, 13–22.
5 M. Ventre, F. Causa and P. A. Netti, *J. R. Soc., Interface*, 2012, **9**, 2017–2032.
6 A. T. Nguyen, S. R. Sathe and E. K. F. Yim, *J. Phys.: Condens. Matter*, 2016, **28**, 183001.
7 K. Anselme, L. Ploux and A. Ponche, *J. Adhes. Sci. Technol.*, 2010, **24**, 831–852.
8 M. Bril, S. Fredrich and N. A. Kurniawan, *Smart Mater. Med.*, 2022, **3**, 257–273.
9 D. Roy, J. N. Cambre and B. S. Sumerlin, *Prog. Polym. Sci.*, 2010, **1–2**, 278–301.
10 S. Municoy, M. I. Álvarez Echazú, P. E. Antezana, J. M. Galdopórpora, C. Olivetti, A. M. Mebert, M. L. Foglia, M. V. Tuttolomondo, G. S. Alvarez, J. G. Hardy and M. F. Desimone, *Int. J. Mol. Sci.*, 2020, **21**, 4724.
11 A. Balcerak-Woźniak, M. Dzwonkowska-Zarzycka and J. Kabatc-Borcz, *Materials*, 2024, **17**, 4255.
12 C. Fedele, P. A. Netti and S. Cavalli, *Biomater. Sci.*, 2018, **6**, 990–995.
13 W. Szymański, J. M. Beierle, H. A. V. Kistemaker, W. A. Velema and B. L. Feringa, *Chem. Rev.*, 2013, **113**, 6114–6178.
14 K. Wu, J. Sun, Y. Ma, D. Wei, O. Lee, H. Luo and H. Fan, *J. Mater. Chem. B*, 2020, **8**, 9212–9226.
15 G. Mayer and A. Heckel, *Angew. Chem., Int. Ed.*, 2006, **45**, 4900–4921.
16 K. G. Yager and C. J. Barrett, Light-Induced Nanostructure Formation using Azobenzene Polymers, in *Polymeric Nanostructures and their Applications*, ed. H. S. Nalwa, American Scientific Publishers, 2006, ch. 8.
17 Z. Mahimwalla, K. G. Yager, J. Mamiya, A. Shishido, A. Priimagi and C. J. Barrett, *Polym. Bull.*, 2012, **69**, 967–1006.
18 D. Liu, Y. Xie, H. Shao and X. Jiang, *Angew. Chem., Int. Ed.*, 2009, **48**, 4406–4408.
19 R. H. Kollarigowda, C. Fedele, C. Rianna, A. Calabuig, A. C. Manikas, V. Pagliarulo, P. Ferraro, S. Cavalli and P. A. Netti, *Polym. Chem.*, 2017, **8**, 3271–3278.
20 L. Rocha, C.-M. Păiuş, A. Luca-Raicu, E. Resmerita, A. Rusu, I.-A. Moleavin, M. Hamel, N. Branza-Nichita and N. Hurduc, *J. Photochem. Photobiol. Chem.*, 2014, **291**, 16–25.
21 M. J. I. Airaghi Leccardi, B. X. E. Desbiolles, A. Y. Haddad, B. C. Joy, C. Song and D. Sarkar, *Commun. Chem.*, 2024, **7**, 249.
22 G. Koçer, J. ter Schiphorst, M. Hendrikx, H. G. Kassa, P. Leclère, A. P. H. J. Schenning and P. Jonkheijm, *Adv. Mater.*, 2017, **29**, 1606407.
23 M. Hendrikx, J. ter Schiphorst, E. P. A. van Heeswijk, G. Koçer, C. Knie, D. Bléger, S. Hecht, P. Jonkheijm, D. J. Broer and A. P. H. J. Schenning, *Small*, 2018, **14**, 1803274.
24 R. M. C. Verbroekken, O. K. Savchak, T. F. J. Alofs, A. P. H. J. Schenning and B. Gumuscu, *ACS Appl. Mater. Interfaces*, 2025, **17**, 27871–27881.
25 A. M. Rosales, K. M. Mabry, E. M. Nehls and K. S. Anseth, *Biomacromolecules*, 2015, **16**, 798–806.
26 K. Homma, A. C. Chang, S. Yamamoto, R. Tamate, T. Ueki and J. Nakanishi, *Acta Biomater.*, 2021, **132**, 103–113.
27 M. Bril, A. Saberi, I. Jorba, M. C. van Turnhout, C. M. Sahlgren, C. V. C. Bouten, A. P. H. J. Schenning and N. A. Kurniawan, *Adv. Sci.*, 2023, **10**, 2303136.
28 P. Rochon, E. Batalla and A. Natansohn, *Appl. Phys. Lett.*, 1995, **66**, 136–138.

29 D. Y. Kim, S. K. Tripathy, L. Li and J. Kumar, *Appl. Phys. Lett.*, 1995, **66**, 1166–1168.
30 R. Kirby, R. G. Sabat, J.-M. Nunzi and O. Lebel, *J. Mater. Chem. C*, 2014, **2**, 841–847.
31 J. Vapaavuori, A. Priimagi and M. Kaivola, *J. Mater. Chem.*, 2010, **20**, 5260–5264.
32 J. Vapaavuori, R. H. A. Ras, M. Kaivola, C. G. Bazuin and A. Priimagi, *J. Mater. Chem. C*, 2015, **3**, 11011–11016.
33 R. Barillé, R. Janik, S. Kucharski, J. Eyer and F. Letournel, *Colloids Surf., B*, 2011, **88**, 63–71.
34 H. W. Baac, J.-H. Lee, J.-M. Seo, T. Park, H. Chung, S.-D. Lee, J. Sung and S. J. Kim, *Mater. Sci. Eng. C*, 2004, **24**, 209.
35 M. Ristola, C. Fedele, S. Hagman, L. Sukki, F. E. Kapucu, R. Mzezewa, T. Hyvärinen, P. Kallio, A. Priimagi and S. Narkilahti, *Adv. Mater. Interfaces*, 2021, **8**, 2100048.
36 C. Rianna, A. Calabuig, M. Ventre, S. Cavalli, V. Pagliarulo, S. Grilli, P. Ferraro and P. A. Netti, *ACS Appl. Mater. Interfaces*, 2015, **7**, 16984–16991.
37 C. Fedele, E. Mäntylä, B. Belardi, T. Hamkins-Indik, S. Cavalli, P. A. Netti, D. A. Fletcher, S. Nymark, A. Priimagi and T. O. Ihalainen, *Sci. Rep.*, 2020, **10**, 15329.
38 M. Isomäki, C. Fedele, L. Kääriäinen, E. Mäntylä, S. Nymark, T. O. Ihalainen and A. Priimagi, *Small Sci.*, 2022, **2**, 2100099.
39 C. Rianna, L. Rossano, R. H. Kollarigowda, F. Formiggini, S. Cavalli, M. Ventre and P. A. Netti, *Adv. Funct. Mater.*, 2016, **26**, 7572–7580.
40 H. Peussa, C. Fedele, H. Tran, M. Marttinen, J. Fadjukov, E. Mäntylä, A. Priimägi, S. Nymark and T. O. Ihalainen, *Adv. Sci.*, 2023, **10**, 2206190.
41 B. Audia, C. Fedele, C. M. Tone, G. Cipparrone and A. Priimagi, *Adv. Mater. Interfaces*, 2022, **9**, 2102125.
42 F. Frascella, A. Angelini, S. Ricciardi, F. Pirri and E. Descrovi, *Opt. Mater. Express*, 2016, **6**, 444–450.
43 J. H. Collier, *Soft Matter*, 2008, **4**, 2310–2315.
44 M. J. Webber, E. A. Appel, E. W. Meijer and R. Langer, *Nat. Mater.*, 2016, **15**, 13–26.
45 F. Mauro, C. F. Natale, V. Panzetta and P. A. Netti, *ACS Appl. Mater. Interfaces*, 2024, **16**(23), 29823–29833.
46 A. J. Nathanael and T. H. Oh, *Polymers*, 2020, **12**, 3061.
47 J. Song, B. Winkeljann and O. Lieleg, *Adv. Mater. Interfaces*, 2020, **7**, 2000850.
48 L. Chen, C. Yan and Z. Zheng, *Mater. Today*, 2018, **21**, 38–59.
49 I. Miranda, A. Souza, P. Sousa, J. Ribeiro, E. M. S. Castanheira, R. Lima and G. Minas, *J. Funct. Biomater.*, 2022, **13**, 2.
50 M. Golda-Cepa, K. Engvall, M. Hakkarainen and A. Kotarba, *Prog. Org. Coat.*, 2020, **140**, 105493.
51 J. Y. Park, S. J. Yoo, E.-J. Lee, D. H. Lee, J. Y. Kim and S.-H. Lee, *BioChip J.*, 2010, **4**, 230–236.
52 J. Raczkowska, S. Prauzner-Bechcicki, J. Lukes, J. Sepitka, A. Bernasik, K. Awsiuk, C. Paluszkiewicz, J. Pabijan, M. Lekka and A. Budkowski, *Appl. Surf. Sci.*, 2016, **389**, 247–254.
53 F. Etezadi, M. N. T. Le, H. Shahsavarani, A. Alipour, N. Moazzezy, S. Samani, A. Amanzadeh, S. Pahlavan, S. Bonakdar, M. A. Shokrgozar and K. Hasegawa, *ACS Biomater. Sci. Eng.*, 2022, **8**, 2040–2052.
54 A. Tooker, E. Meng, J. Erickson, Y.-C. Tai and J. Pine, *IEEE Eng. Med. Biol. Mag.*, 2005, **24**, 30–33.
55 T. Y. Chang, V. G. Yadav, S. De Leo, A. Mohedas, B. Rajalingam, C.-L. Chen, S. Selvarasah, M. R. Dokmeci and A. Khademhosseini, *Langmuir*, 2007, **23**, 11718–11725.
56 S. Gholizadeh, D. M. Lincoln, Z. Allahyari, L. P. Widom, R. N. Carter and T. R. Gaborski, *Sci. Rep.*, 2023, **13**, 4262.
57 C. P. Tan and H. G. Craighead, *Materials*, 2010, **3**, 1803–1832.
58 U. Eduok, O. Faye and J. Szpunar, *Prog. Org. Coat.*, 2017, **111**, 124–163.
59 K. M. F. Rossi de Aguiar, M. V. Nascimento, J. L. Faccioni, P.-L. M. Noeske, L. Gätjen, K. Rischka and U. P. Rodrigues-Filho, *Appl. Surf. Sci.*, 2019, **484**, 1128–1140.
60 P. L. Gourley, R. G. Copeland, J. D. Cox, J. K. Hendricks, A. E. McDonald, S. L. Peterson and D. Y. Sasaki, *J. Biomed. Opt.*, 2002, **7**, 546–554.
61 M. Cieślik, K. Engvall, J. Pan and A. Kotarba, *Corros. Sci.*, 2011, **53**, 296–301.
62 M. Cieślik, S. Zimowski, M. Gołda, K. Engvall, J. Pan, W. Rakowski and A. Kotarba, *Mater. Sci. Eng., C*, 2012, **32**, 2431–2435.
63 J. Ortigoza-Diaz, K. Scholten, C. Larson, A. Cobo, T. Hudson, J. Yoo, A. Baldwin, A. Weltman Hirschberg and E. Meng, *Micromachines*, 2018, **9**, 422.
64 B. J. Kim and E. Meng, *Polym. Adv. Technol.*, 2016, **27**, 564–576.
65 C. Hassler, R. P. von Metzen, P. Ruther and T. Stieglitz, *J. Biomed. Mater. Res., Part B*, 2010, **93B**, 266–274.
66 L. Brancato, D. Decrop, J. Lammertyn and R. Puers, *Materials*, 2018, **11**, 1109.
67 G. E. Loeb, M. J. Bak, M. Salcman and E. M. Schmidt, *IEEE Trans. Biomed. Eng.*, 1977, **BME-24**, 121–128.
68 X. Z. Xie, L. Rieth, P. Tathireddy and F. Solzbacher, *Proc. Eng.*, 2011, **25**, 483–486.
69 H. C. Koydemir, H. Külah and C. Özgen, *J. Microelectromech. Syst.*, 2014, **23**, 298–307.
70 E. Song, R. Li, X. Jin, H. Du, Y. Huang, J. Zhang, Y. Xia, H. Fang, Y. K. Lee, K. J. Yu, J.-K. Chang, Y. Mei, M. A. Alam, Y. Huang and J. A. Rogers, *ACS Nano*, 2018, **12**, 10317–10326.
71 A. Laventure, A. Soldera, C. Pellerin and O. Lebel, *New J. Chem.*, 2013, **37**, 3881–3889.
72 A. Goulet-Hanssens, T. C. Corkery, A. Priimagi and C. J. Barrett, *J. Mater. Chem. C*, 2014, **2**, 7505–7512.
73 W. F. Gorham, *J. Polym. Sci.*, 1966, **4**, 3027–3039.
74 Y. Liu, D. Kang, W. Dai, H. Li, W. Wang and Y.-C. Tai, *Micro Nano Syst. Lett.*, 2018, **6**, 5.
75 A. Santiago-Alvarado, A. Cruz-Felix, F. Iturbide and B. Licona-Morán, *Int. J. Eng. Sci. Innov. Technol.*, 2014, **3**, 563–571.
76 P. Bai, M. Ma, L. Sui and Y. Guo, *J. Phys. Chem. Lett.*, 2021, **12**, 8072–8079.

77 Z. Ao and S. Li, *Nanoscale Res. Lett.*, 2011, **6**, 243.
78 Y. Wyser, C. Pelletier and J. Lange, *Packag. Technol. Sci.*, 2001, **14**, 97–108.
79 R. A. Nawrocki, *Adv. Funct. Mater.*, 2019, **29**, 1906908.
80 C. Hubert, C. Fiorini-Debuisschert, I. Maurin, J.-M. Nunzi and P. Raimond, *Adv. Mater.*, 2002, **14**, 729–732.
81 H. Leblond, R. Barille, S. Ahmadi-Kandjani, J.-M. Nunzi, E. Ortyl and S. Kucharski, *J. Biomed. Mater. Res., Part B*, 2009, **42**, 205401.
82 L. Mazaheri, R. G. Sabat, O. Lebel and J.-M. Nunzi, *Opt. Mater.*, 2016, **62**, 378–391.
83 A. Takei, L. Jin, H. Fujita, A. Takei, H. Fujita and L. Jin, *ACS Appl. Mater. Interfaces*, 2016, **8**, 24230–24237.
84 H. Rekola, A. Berdin, C. Fedele, M. Virkki and A. Priimagi, *Sci. Rep.*, 2020, **10**, 19642.
85 A. Berdin, H. T. Rekola and A. Priimagi, *Adv. Opt. Mater.*, 2024, **12**, 2301597.
86 N. Chou, H. Moon, J. Park and S. Kim, *Prog. Org. Coat.*, 2021, **157**, 106309.
87 A. J. Nolte, J. Y. Chung, C. S. Davis and C. M. Stafford, *Soft Matter*, 2017, **13**, 7930–7937.
88 R. Huang and Y. C. Tai, in *TRANSDUCERS 2009 - 2009 International Solid-State Sensors, Actuators and Microsystems Conference*, 2009, pp. 1027–1030.
89 J. Charmet, J. Bitterli, O. Sereda, M. Liley, P. Renaud and H. Keppner, *J. Microelectromech. Syst.*, 2013, **22**, 855–864.
90 J. Ortigoza-Diaz, K. Scholten and E. Meng, *J. Microelectromech. Syst.*, 2018, **27**, 874–885.
91 R. P. von Metzen and T. Stieglitz, *Biomed. Microdevices*, 2013, **15**, 727–735.
92 J. Vapaavuori, V. Valtavirta, T. Alasaarela, J.-I. Mamiya, A. Priimagi, A. Shishido and M. Kaivola, *J. Mater. Chem.*, 2011, **21**, 15437–15441.
93 J. E. Koskela, J. Vapaavuori, R. H. A. Ras and A. Priimagi, *ACS Macro Lett.*, 2014, **3**, 1196–1200.
94 S. Vesamäki, H. Meteling, R. Nasare, A. Siiskonen, J. Patrakka, N. Roas-Escalona, M. Linder, M. Virkki and A. Priimagi, *Commun. Mater.*, 2024, **5**, 1–11.
95 G. Mehta, J. Lee, W. Cha, Y.-C. Tung, J. J. Linderman and S. Takayama, *Anal. Chem.*, 2009, **81**, 3714–3722.
96 W. Chun, N. Chou, S. Cho, S. Yang and S. Kim, *Prog. Org. Coat.*, 2014, **77**, 537–547.
97 J. G. Gluschke, F. Richter and A. P. Micolich, *Rev. Sci. Instrum.*, 2019, **90**, 083901.
98 C. M. McGrath and P. B. Blair, *Cancer Res.*, 1970, **30**, 1963–1968.
99 C. M. McGrath, *Am. Zool.*, 1975, **15**, 231–236.
100 J. E. Lever, *Proc. Natl. Acad. Sci. U. S. A.*, 1979, **76**, 1323–1327.
101 A. I. Teixeira, G. A. Abrams, P. J. Bertics, C. J. Murphy and P. F. Nealey, *J. Cell Sci.*, 2003, **116**, 1881–1892.
102 J. M. Anderson, B. R. Stevenson, L. A. Jesaitis, D. A. Goodenough and M. S. Mooseker, *J. Cell Biol.*, 1988, **106**, 1141–1149.
103 E. McNeil, C. T. Capaldo and I. G. Macara, *Mol. Biol. Cell*, 2006, **17**, 1922–1932.
104 Y. J. Chuah, S. Kuddannaya, M. H. A. Lee, Y. Zhang and Y. Kang, *Biomater. Sci.*, 2015, **3**, 383–390.
105 Y. J. Chuah, Y. T. Koh, K. Lim, N. V. Menon, Y. Wu and Y. Kang, *Sci. Rep.*, 2015, **5**, 18162.
106 S. H. Tan, N.-T. Nguyen, Y. C. Chua and T. G. Kang, *Biomicrofluidics*, 2010, **4**, 032204.
107 S. L. Peterson, A. McDonald, P. L. Gourley and D. Y. Sasaki, *J. Biomed. Mater. Res. A*, 2005, **72A**, 10–18.
108 K. Ma, J. Rivera, G. J. Hirasaki and S. L. Biswal, *J. Colloid Interface Sci.*, 2011, **363**, 371–378.
109 L. Kääriäinen, *BSc thesis*, Tampere University, 2022. Available from: **https://urn.fi/URN:NBN:fi:tuni-202201031009**.